Damage-based assessment of the risk of cut-out in trochanteric fractures for different PFNA blade positions

Francisco Maria Serra Rebelo de Andrade
franciscorebelodeandrade@tecnico.ulisboa.pt

Instituto Superior Técnico, Universidade de Lisboa, Portugal

November 2021

Abstract

Cut-out of the hip screw of fracture fixation implants, defined as the perforation of the femoral head by the screw due to the collapse of the neck-shaft angle into varus, is the most common mechanical complication in the treatment of trochanteric fractures. Among the factors that contribute to cut-out, the blade positioning in the femoral head is reported as one of the most relevant. Since the optimal blade position in the superior-inferior and medial-lateral directions is unknown, the goal of this work was to investigate the impact of blade positioning in these directions, using three-dimensional finite element models of two femora with unstable trochanteric fractures and eight different screw positions. These models were coupled with a stiffness-adaptive damage model for the evaluation of the risk of cut-out. The PFNA blade was placed in each model at four discrete distances from the femoral head surface – 5, 10, 15 and 20 mm – in both central and inferior positions. The damage distribution in bone resulting from a gait loading condition was visually and quantitatively assessed to compare the performance of the eight positions and predict the relative risk of cut-out for each. The results suggest that the deeper the blade, the lower the risk, although no tip-surface distances under 5 mm are recommended, and that the medial-lateral position is more relevant as a cut-out predictor than the superior-inferior position. Excessive loading conditions were also evaluated and were found to greatly impact the risk of cut-out.

Keywords: Cut-out, Damage, Finite Element Method, PFNA, Trochanteric fractures

1. Introduction

Hip fractures are a common health problem among the elderly population all over the world, mainly due to the increasing aging of population and the prevalence of osteoporosis. These fractures present the highest rates of morbidity and mortality of all osteoporotic fractures. The main cause of hip fractures is low-impact trauma resulting from falls, representing 90-92% of fractures, and female patients are the most affected. It has been reported that approximately 20% of the patients die within 1 year of the fracture, and that only 40-79% regain their previous ambulatory function a year after the fracture, with less than half returning to their pre-fracture status of independence and daily activities [1–3].

Hip fractures occur on the proximal part of the femur, and may be divided into intracapsular or extracapsular, with the latter being subdivided into trochanteric and subtrochanteric fractures. They are influenced by hip anatomy, the hip joint forces and bone mechanical properties. The treatment of hip fractures is mainly surgical, representing a large part of the orthopedic surgery activity, and have associated high clinical and social cost implications. For most cases, fractures are stabilized using either intra- or extramedullary fixation devices, generally composed of a rod placed along the femoral shaft and a screw or a blade crossing the femoral head; the most common are, respectively, the Proximal Femoral Nail Antirotation (PFNA) and the Dynamic Hip Screw (DHS). Although allowing a stable fixation in the majority of cases, there is still a significant number of post-operative complications reported, compromising the success of the procedure. The hip screw cut-out, defined as the collapse of the neck-shaft angle into varus leading to extrusion of the screw from the femoral head, is the most common mechanical complication, accounting for 85% of fixation failures. Other common complications have to do with mal-union or non-union of the fracture fragments, femoral shaft fracture or implant failure. Several factors may affect the risk of cut-out, including the patient's age and sex, bone quality, fracture pattern and stability, quality of reduction, the neck-shaft angle of the fixation device and its design, and the screw positioning in the femoral

head [1, 4–7].

While the screw position has been frequently discussed in the literature, there is no clear consensus yet about the optimal position to reduce the risk of cut-out [7]. Many clinical studies evaluated the position of the screw immediately after the surgery and after a follow-up period, performing statistical studies to find relations between the post-surgical position and the risk of cut-out [8–12]. On the other hand, computational studies have been using finite element models for different screw positions, evaluating mainly the stress and strain distribution to conclude about the position that leads into less bone damage [6, 13–17]. While it is consensual that the central position in the anterior-posterior direction is the less prone to cut-out, findings about the position in the other directions are contradictory. In the superior-inferior direction, literature conclusions are divided between central and inferior positions. For the medial-lateral directions, while there are few studies that focus on the position in this direction, surgical technical guides suggest a 10 mm direction between the tip of the screw and the femoral head surface, measured in a straight line along the axis of the screw. Baumgaertner et al. [18] have proposed a measure, the tip-apex distance (TAD) – the distance from the tip of the screw and a point in the femoral head surface, measured in both anteroposterior and lateral views – to evaluate the risk of cut-out, arguing that a lower TAD led to a lower risk. However, while some authors supported this finding, others have shown opposition to it.

The goal of this work is to contribute to the investigation on the optimal position for the PFNA blade in the superior-inferior and medial-lateral directions, using three-dimensional finite element models of two femora with unstable trochanteric fractures and eight different screw positions, varying both the superior-inferior position and the depth of insertion of the screw. These models were coupled with a damage model for the evaluation of the risk of cut-out. Another goal is to study the influence of the loading intensity on the risk of cut-out.

2. Methods

2.1. Damage model

A quasi-brittle damage model based on continuum damage mechanics was used in this work. This model, based on a work by Hambli et al. [19], uses an isotropic behaviour law coupled to a quasi-brittle damage law to describe the damage evolution on the bone and its influence on the structural stiffness reduction. A damage variable D is defined, which acts as a stiffness reduction factor: its value ranges between 0 (no damage, no loss of stiffness) and 1 (total damage, total loss of stiffness). Considering the damage value, the effective Young's modulus, E, is given in function of the undamaged Young's modulus, E_0, by:

$$E = (1 - D)\, E_0 \tag{1}$$

The damage parameter evolves according to a power law when the equivalent strain, given by

$$\varepsilon_{eq} = \sqrt{\frac{2}{3}\,\varepsilon_{ij}\,\varepsilon_{ij}} \tag{2}$$

is between the yield strain, ε_0, and the strain at fracture, ε_f, above which the material loses all stiffness. Damage growth may occur until the damage parameter reaches the critical damage value, D_c, where all stiffness is lost. The damage law is given by:

$$D = \begin{cases} 0 & ;\ \varepsilon_{eq} \leq \varepsilon_0 \\ D_c \left(\dfrac{\varepsilon_{eq}}{\varepsilon_f}\right)^n & ;\ \varepsilon_0 < \varepsilon_{eq} < \varepsilon_f \\ D_c & ;\ \varepsilon_{eq} \geq \varepsilon_f \end{cases} \tag{3}$$

Damage growth is controlled by a function $f(\varepsilon_{eq}, \varepsilon_0) = \varepsilon_{eq} - max(k, \varepsilon_0)$, where $k = \max(\varepsilon_{eq})$ is the maximum equivalent strain reached during loading history. This condition implies that damage cannot decrease.

The damage model handles differently tension and compression, having different values of parameters ε_0, ε_f and D_c for both cases. The differentiation is based on the hydrostatic stress. Table 1 presents the damage model parameters for both tension (T) and compression (C).

Table 1: Damage model parameters. The first line presents the values, while the second line indicates the source.

n	D_c^T	ε_0^T	ε_f^T	D_c^C	ε_0^C	ε_f^C
2	0.95	0.7%	2.5%	0.5	1.04%	4.0%
[20]	[19]	[21]	[19]	[19]	[21]	[19]

2.2. Finite element model

Three-dimensional geometric models of a male and a female right femora, provided by Quental et al. [17], were used as the basis for this work. These femora were generated from sets of CT images, using software ITK-SNAP (version 3.8.0, 2019). An unstable fracture classified as 31-A2.2 in the Müller AO classification system was modelled in Solidworks (2020 version) from an anteroposterior view, with an angle of 43°between the fracture line and the femoral shaft axis [22], an intrusion distance of

95% of the fracture line length[1], and an opening angle of 6.5°. The fracture divided the bone model into 2 parts: a superior part (SP), including the femoral neck and head, and an inferior part (IP), including the femoral shaft. The fracture fragments were not included in the model. The PFNA implant was also modelled in Solidworks, according to the geometries and dimensions provided by DePuy Synthes in the surgical technique guide [23]. The assembly of the components was performed following the guidelines of the surgical technique guide, with the blade being placed in eight different positions: for central and inferior positions in the superior-inferior direction, distances from the tip of the blade to the femoral head surface of 5, 10, 15 and 20 mm were considered. For all configurations, the blade was placed centrally in the anterior-posterior direction, since it has been widely reported in the literature that this position reduces the risk of cut-out [8–12]. Figure 1 shows the 8 assembly configurations modelled for the female bone. Henceforth, and for the sake of simplicity, each geometry is referred to by a code starting with the letter M or F (whether the model is of the male or female femur, respectively), followed by "inf" for central-inferior positions and "cent" for central-central positions, and by the distance, in milimetres, from the tip of the blade to the external surface of the femoral head (e.g. Minf5, Fcent20).

Isotropic, linear elastic materials were assigned to all components of the models. The implant is made of a titanium alloy (Ti-6Al-7Nb), with a Young's modulus $E = 105$ GPa and a Poisson's ratio $\nu = 0.3$. Bone was modelled as an inhomogeneous material, with its Young's modulus varying punctually with density. The density distribution was obtained for the intact bone models from the CT images using an Abaqus plug-in called Bonemapy. The density range was defined as 0.01-1.32 g cm^{-3}, which are typical density values for osteoporotic bones, because these fractures tend to occur mostly in the elderly population [17, 24]. To avoid inaccuracy resulting from partial volume effects on the obtainment of densities, two shells reproducing the external surfaces of the SP and IP were modelled, representing the external cortex. These shells were assigned a Young's modulus of 10.37 GPa, corresponding to the Young's modulus of the maximum bone density considered, and a thickness of 0.5 mm [25, 26]. An in-house MATLAB program was used to map the densities and convert the density distribution to the fractured model. For each node on the new model, this program defined its density: (i) equal to the density of a node on the original model, if the coordinates of both nodes were the same, or (ii) as a weighted average, with the inverse of the square of the distance, of the nodes on the original model with the closest coordinates. The relationship between Young's modulus and bone density, ρ, for each point of the bone, is given by [27]:

$$E_0 = 6850\,\rho^{1.49} \tag{4}$$

The interactions defined in Abaqus between parts were of two types: tie constraints and surface-to-surface contact interactions. The outer cortical bone shells were tied to the bone. A tie constraint was also defined between the distal locking screw and the bone. Despite not being representative of the real contact, this approximation was made for the sake of simplicity, since this contact is expected to have little impact on the results.

The other interactions were defined as surface-to-surface contact. There are 3 types of surface interactions: bone-bone, bone-implant, and implant-implant. The bone-bone interaction between the superior and inferior parts of the bone considered a friction coefficient of 0.46 [5]. The interactions between the bone and the nail and between the bone and the blade considered a friction coefficient of 0.3 [5]. Finally, the implant-implant interactions, defined between the nail and both the blade and the locking screw, had a friction coefficient of 0.2 [28].

The loading conditions were defined to simulate the forces acting on the femur during gait. According to Heller et al. [29], the forces on the proximal femur during walking are applied on 3 points, designated as P_0, P_1 and P_2. This points represent, respectively, the hip contact point on the femoral head; the point where the abductor muscles and the tensor fascia latae act, located on the lateral region of the greater trochanter; and a point on the lateral region below the line of the lesser trochanter where the vastus lateralis attaches. The attachment points locations are represented in figure 2. All these 3 points were defined in Abaqus as Attachment Points, and were coupled to shell areas on their vicinity using Coupling constraints, so that each applied force was distributed by a number of nodes, avoiding high punctual stresses. The distribution of the force on point P_0 was defined to be quadratic over the slave surface, by defining the coupling type as continuum distributing with a quadratic weighting method, while the forces acting on points P_1 and P_2 were distributed according to a uniform weighting method [25]. Heller et al. [29] present the load values as percentages of the bodyweight, which are shown in Table 2. The conversion of the loads to the actual values in Newton was made considering masses of 90.8 kg and 75.5 kg for the male and female subjects, respectively. The loads are given in the coordinate system described

[1]Representative of a 31-A2.2 fracture based on clinical guidance from Dr. Francisco Guerra Pinto, from Sant'Ana Orthopaedic Hospital.

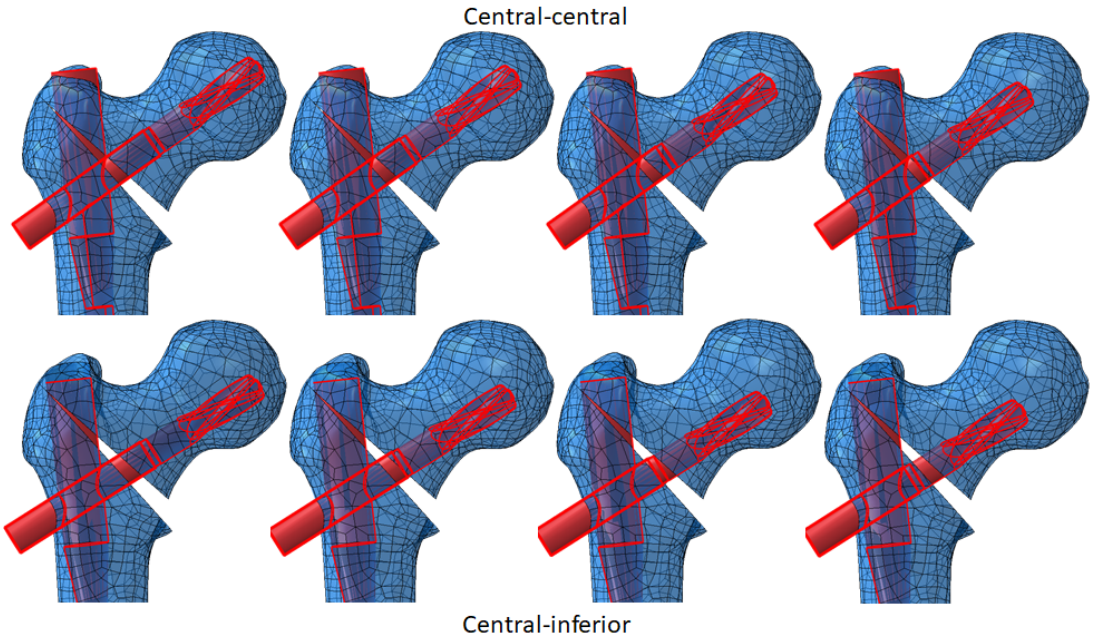

Figure 1: Representation of the eight configurations of the implant on the female bone. From left to right: distances of 5 mm, 10 mm, 15 mm and 20 mm from the tip of the blade to the external surface of the femoral head.

by Bergmann et al. [30], which aligns its z axis with the femoral shaft axis. To prevent rigid body motion, the base of the femur was constrained using an encastre condition.

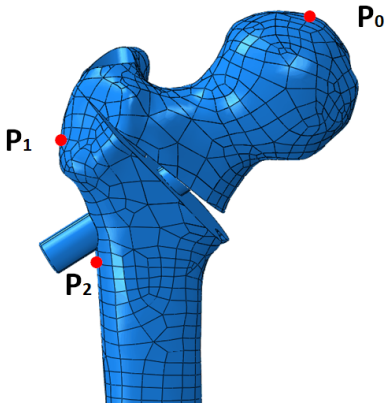

Figure 2: Attachment points for the application of loads in the female model.

Finally, the finite element mesh was generated. The 3D solid parts – bone and implant – were discretized using quadratic tetrahedral elements (C3D10), due to the complexity of the structures, particularly the bone parts. The bidimensional shell parts were discretized with quadratic triangles (STRI65). Mesh sizes were defined following Quental et al. [17], who performed a convergence analysis to select a proper element size for the mesh. The convergence was assessed based on the evolution of the minimum principal strain on 3 nodes of the model with the element size. They concluded that the optimal element size to satisfy both convergence and computational efficiency was 2 mm for the SP and 3 mm for the IP and the implant.

Table 2: Loads acting on the proximal femur, in percentage of bodyweight (adapted from [29]). TFL is short for the muscle tensor fascia latae.

	F_x	F_y	F_z	Point
Hip contact	54.0	-32.8	-229.2	P0
Abductor	-58.0	4.3	86.5	P1
TFL, proximal	-7.2	11.6	13.2	P1
TFL, distal	0.5	-0.7	-19.0	P1
Vastus lateralis	0.9	18.5	-92.9	P2

2.3. Damage model and FEM integration

The developed finite element models presented in Section 2.2 were coupled with the damage model described in Section 2.1. The domain was discretized by the FE model, and the damage model was applied locally to each node of the bone, using the equations in Section 2.1. Stresses and strains were computed through FE analyses. The application of the damage model equations provides a nodal damage distribution for both the SP and IP of the bone. This damage distribution affects the Young's modulus distribution, but only takes effect on a next FE analysis. This requires the implementation of an it-

erative procedure. Three different load application strategies for the simulations were considered: (i) loads were gradually incremented using loads steps (for example, starting with 25% of load, 25% load increments were applied after each iteration until all load was applied); (ii) full loading was initially applied but several iterations were performed until the damage distribution changed less than a predefined threshold; (iii) loads were gradually incremented, as in (i), and several iterations were performed after reaching full load until damage changed less than a predefined threshold, as in (ii). Henceforth, for the sake of simplicity, strategy (i) is referred to as incremental loading strategy, strategy (ii) as full loading strategy and strategy (iii) as hybrid strategy.

The convergence criterion for the full loading strategy was based on the variation of a parameter internally named DIVol, that is a measure that combines the volume of bone with damage to the actual damage value on each point. To obtain DIVol, which corresponds to the integral of the damage distribution over the total bone volume, the finite element method was used. Resorting to Gauss integration:

$$\mathrm{DIVol} = \sum_{e=1}^{\mathrm{NE}} \sum_{i=1}^{\mathrm{NIP}} D_i^e \, \mathrm{IVol}_i^e \tag{5}$$

where NE is the number of elements of the bone mesh, NIP is the number of integration points per element, which is 4 for C3D10 elements, and IVol is the volume associated to each integration point. For each iteration, a convergence parameter (CP) was computed as the relative deviation of DIVol between the current and previous iterations.

The bone material model was adapted to include the stiffness reduction, as described in Eq. 1. According to the damage model, a node under critical damage conditions would have a null Young's modulus. However, as a way of avoiding numerical instabilities, a low Young's modulus of 0.01 MPa was considered [31]. In some cases, the minimum stiffness was too small, causing convergence problems. To overcome these convergence problems, the minimum stiffness was updated to 0.1 MPa whenever convergence problems arose. A sensitivity analysis was performed for the minimum stiffness value to make sure that this procedure had little impact on the results.

An code was developed in MATLAB to implement the algorithm. It starts by reading the loads, nodal densities and model parameters (cf. table 1), along with data for the algorithm, namely the convergence tolerance for the full loading strategy and the number of steps for the incremental loading strategy. If the incremental loading strategy is to be performed, a *for* cycle, with the previously defined number of steps, is initiated. This cycle starts by incrementing the loads for the new load step. The FEA is performed and the results necessary for the damage model - stresses and strains - are extracted. The damage model is applied to each node of the bone, and the resulting nodal damage is written to a file. This repeats until the number of iterations performed matches the number of load steps previously defined. The full loading strategy, that can occur after the incremental loading (for the hybrid strategy) or independently, starts by setting full loading. The next steps are similar to the ones happening on the incremental loading strategy, from running the FEA to writing the damage and α files. At the end of each iteration, parameter DIVol and the convergence parameter are computed. The cycle starting on the FEA execution is repeated until the convergence parameter is below the tolerance previously defined.

2.4. Analysis of the risk of cut-out

Several authors have assumed a relation between the volume of yielded bone and the risk of cut-out [16,17,32]. Goffin et al. [16] evaluated only the superior part of the bone (SP), stating that cut-out is likely to occur due to high compressive strains in the whole head and neck regions. In order to take advantage of having a damage model differentiating the damage intensity, a new parameter was developed to evaluate the risk of cut-out. This parameter, named DIVol-SP, was computed like DIVol (cf. Equation 5), but only included the superior part of the bone. DIVol-SP works like a weighted volume that allows for nodes with higher damage to be considered more than those with a lower damage value.

To evaluate the influence of the superior-inferior and medial-lateral positions of the blade, simulations were performed for the eight configurations presented in figure 1, for both the female and male models.

The influence of higher loading conditions in the damage evolution, intending to represent incidents, was also investigated. Simulations with double the loads proposed by Heller et al. [29] were performed. Because of limited computational capacity, it was not possible to perform simulations for all models; therefore, models Finf5 and Fcent20 were chosen, since they represent, according to Quental et al. [17], the safest and least safe positions of the female model.

3. Results

The results obtained were qualitatively compared with those of Quental et al. [17], showing similar damaged zones in the bone, which provided confidence in the correct implementation of the damage model used. The load application strategies referred in Section 2.3 were compared with the aim

of choosing the best one to implement in this work. The results obtained using the incremental loading strategy were found to depend substantially on the number of steps chosen, with no sign of result convergence for computationally efficient numbers of steps – this strategy was therefore excluded. The full loading and hybrid strategies were compared for a male and a female model. The resulting damage distributions were found to be similar, as well as the values of DIVol. Considering that, for this work, only the final damage distribution is relevant, the selection of the loading strategy was made based on the most computationally efficient, which was the full loading strategy.

3.1. Assessment of the risk of cut-out

Figure 3 presents the damage distribution resulting from the gait load case for all geometries of the female and male models. In both central-central and central-inferior positions, three main regions tended to be critical: at the tip of the blade; around the region where the blade transitions from a cylindrical shape to a helical shape; and at the contact regions immediately above and below the fracture. Also, comparing the positions along the medial-lateral directions, damage increased with the distance to the femoral head surface in the three regions.

Figure 4 presents the DIVol for both the SP and IP of all geometries for both the female and male models, for qualitative comparison of the bone damage.

The effect of a loading intensity above normal was also evaluated for the Finf5 and Fcent20 models. For the sake of briefness only the results for the Finf5 are shown in this paper, since they could easily be extrapolated for other geometries. Figure 5 presents the damage distribution for the Finf5 model with the normal loading scheme and with a 100% overload. The damage distribution follows the same pattern, albeit with a higher incidence. DIVol-SP was 207.12 on the normal load case, and 4361.2 on the overload case. These values represent, respectively, 26.4% and 57.5% of the total DIVol of the models.

4. Discussion

To gain confidence on the damage model behaviour, the results were compared to those of Quental et al. [17]. The damage distribution was consistent with the regions with strain above the yield strain of these works, providing confidence in the damage model implementation. The residual differences on both distributions may be attributed to different yielding criteria used: while Quental et al. evaluated the minimum (compressive) principal strains, this work used an equivalent strain to take into consideration the total strain at each node; also, the yield strains considered were different.

Although a central position in the anterior-posterior direction is consensually optimal for the positioning of the PFNA blade, no consensus exists yet on the best position in the superior-inferior direction. Arias-Blanco et al. [6], Hsueh et al. [9] and Konya et al. [33] defended that the blade should be placed centrally, while Lee et al. [13], Quental et al. [17] and Celik et al. [14] recommended an inferior position. From the results obtained for the female model, the inferior position was less prone to cut-out, since the DIVol-SP was lower than in the central positions for the same depth. For the male model, the central positions seemed safer than the inferior positions. This may be explained by differences in their density distribution. For the female model, the blade was always positioned in regions of low bone density, whereas for the male model, the central positioning of the blade placed it in a region of higher bone density than when placed inferiorly. This may explain the higher safety in central positions suggested by the results for the male femur.

The depth of placement of the blade was found to greatly influence the decrease of the risk of cut-out. For both male and female models, results suggested that the higher the distance from the tip of the blade to the external surface of the femoral head, the higher the damage in the three main regions to be evaluated in the SP: at the tip of the blade; in the blade transition region; and in the fracture region. These are the same regions identified by Goffin et al. [16] and Quental et al. [17] as critical for the risk of cut-out. The visual inspection of damage distribution (cf. Figure 3) and the evolution of the DIVol-SP with the distance (cf. Figure 4) confirm the influence of the depth of the blade position on the risk of cut-out. This conclusion is verified for both central and inferior positions, partially contradicting the findings of Vasconcelos [32], who found no damage at the tip of the blade and around the blade transition region for central geometries and argued that, for these geometries, no significant differences on the risk of cut-out were observed, suggesting that orthopaedic surgeons have a margin for error if the blade is inserted in this position. Based in the results obtained, the recommended depth of the blade is 5 mm. There are other effects that were not taken into consideration in this study, in particular medial perforations of the proximal femur [34]. Therefore, positioning the blade with a distance under 5 mm is not recommended, since this is the minimum suggested distance by the manufacturer [23].

Regarding the global blade positioning, while the results suggest inserting the blade as deep as possible, they are unable to identify which position is best along the superior-inferior direction. Nevertheless, from Figure 4, the difference of the risk of

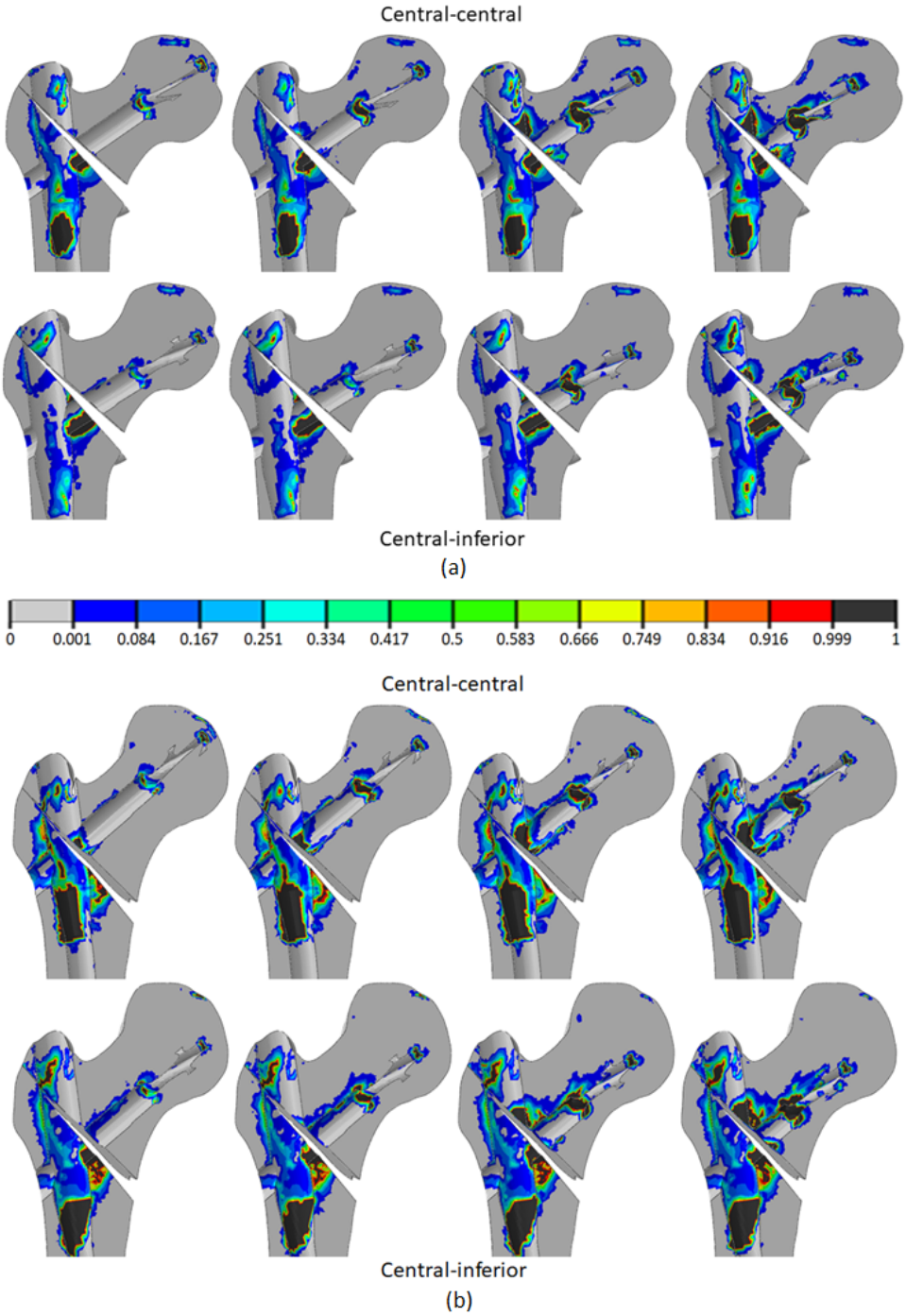

Figure 3: Damage distribution on the (a) female and (b) male bone models. From left to right, distances from the tip of the blade to the femoral head surface of 5, 10, 15 and 20 mm.

cut-out for different depths is higher than that for different superior-inferior positions. Also, using as example the female case results, a deep central position is less prone to cut-out than a less deep inferior position. These considerations suggest that the depth of the blade position is a more relevant indicator for the risk of cut-out than the blade position in the superior-inferior direction.

Unlike Quental et al. [17], the male models were found to present a higher risk of cut-out, having, for the same blade positions, higher DIVol than the female bones. Despite being discrepant, these results are supported by the literature, where there is generally no relationship reported between the patient's sex and the propensity to cut-out [35, 36].

The new fracture modelled in this work repre-

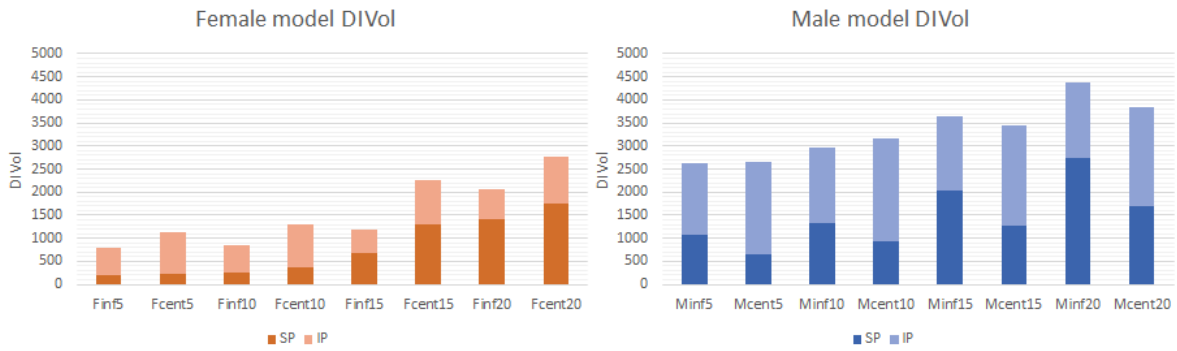

Figure 4: DIVol for both the SP and IP of all geometries.

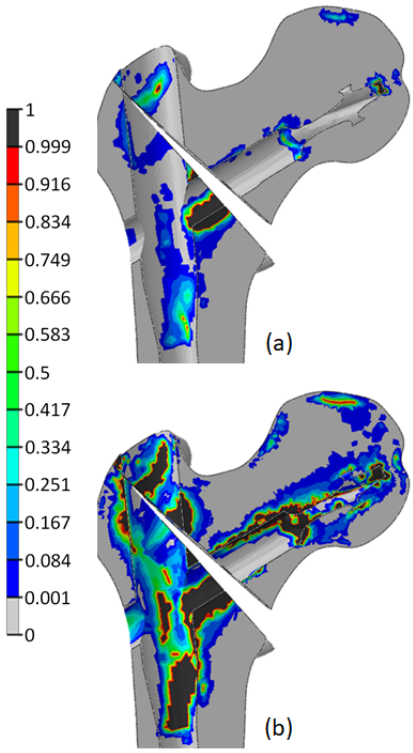

Figure 5: Comparison between the damage distribution on the Finf5 model using the (a) normal loading scheme or (b) a 100% overload.

sents a poorer reduction of the fracture than those of Goffin et al. [16] and Quental et al. [17], introducing more instability in the system and a higher risk of cut-out [37]. This fracture geometry has not been mentioned previously in the literature, for what this work represents an advance in the studies of different trochanteric fractures.

The overload analyses showed a significant increase in the risk of cut-out. DIVol-SP increased 21 times in the Finf5 case with a 100% load increment, and the percentage of DIVol-SP relative to the total DIVol went from 26.4% to 57.5%, more than duplicating – suggesting that, with excessive loading, the SP starts to gain more preponderance on the damage distribution over the IP. The overload analyses intended to evaluate incidents happening to the patients – while Heller et al. [29] loading conditions are a good approximation of the real forces exerted during gait under normal conditions, incidents that are responsible for high impact (e.g. falls) may happen, leading to more severe loading in the proximal femur. Figure 5 presents damage above the entire length of the blade for the high load results, indicating the propensity of the femoral head to move down relatively to the screw, leading to a higher risk of the screw to cut-out of the superior region of the femoral head.

Despite its contributions, this work contains some limitations. Firstly, from a geometric point of view, only one female and one male femora were studied, with only one fracture geometry. Although the study would have benefited from having more femur models, the analysed femora fall within the typical geometries [17]. Nevertheless, different fracture geometries would have allowed to perceive the influence of this factor in the results. Regarding loading, only one loading case, representative of gait, was implemented in this work, limiting its applicability to everyday situations.

Regarding the implementation of the models, the damage model was only applied to the solid bone parts; nonetheless, since the shells are also bone tissues, the damage model could have been applied to these structures as well. Furthermore, other works implemented this damage model in Abaqus/Standard using a subroutine UMAT [19], while, in this work, the damage model was implemented using a MATLAB routine. Using UMAT allows for the damage model to be implemented directly in every increment of the Abaqus' Step, while the present approach computed damage only at the end of the step. With UMAT, the stiffness is updated several times in the same iteration, while, with the present implementation, the stiffness for

a given iteration is constant [38]. Finally, the same works used an element deletion technique when critical damage was reached, allowing for the fracture to progress. In this work, the critical damaged nodes were maintained, with its Young's modulus only being reduced.

5. Conclusions

The goal of the present work was to assess the risk of cut-out for several positions of the PFNA blade on the femoral head. To accomplish that, 3D finite element models for both a female and a male femora treated with PFNA implants were coupled with a quasi-brittle stiffness-adaptive damage model to evaluate the bone damage resulting from the loading conditions from gait. The PFNA blade was placed in eight different positions, varying both the superior-inferior and medial-lateral positions, in order to assess the effect of each position in the bone damage distribution. To the author's knowledge, this is the first study to apply a damage model with stiffness adaptation to assess of the risk of cut-out in a bone-implant system of a hip fracture.

Overall, the depth of placement of the blade in the medial-lateral direction and its superior-inferior position were shown to have great influence in the risk of cut-out, with the medial-lateral position being the most relevant predictor. The best position to place the blade was found to be in the inferior (for the female bone) or central (for the male bone) regions, at a 5 mm distance from the femoral head surface. Bone critical damage was found to be predominant at the tip of the blade, around the blade's transition region and at the fracture region. Finally, the influence of higher loads than usual was found to represent a greater risk of cut-out.

To the author's knowledge, this is the first study to apply a damage model to a bone-implant system of a hip fracture, leading bone stiffness to be constantly adapting according to the damage distribution, and allowing the identification of the most critical areas on the bone. Nonetheless, some work remains to be done.

A larger number of femora should be considered in future studies. This would allow to investigate the reason behind the contradictory results for the two femora considered regarding the superior-inferior position. Also, different fracture geometries should be studied, to evaluate its influence in the recommended blade position and the risk of cut-out. Different loading cases should also be analysed (e.g. stair climbing), in order to have a broader knowledge on the risk of cut-out for everyday situations. Finally, concerning the implementation of the damage model, a kill-element technique could be implemented, in order to allow microcracks to progress.

References

[1] M. N. Sarvi. Hip fracture: Anatomy, causes, and consequences. *IntechOpen*, November 2018. doi: 10.5772/intechopen.75946.

[2] E. K. Osnes, C. M. Lofthus, H. E. Meyer, J. A. Falch, L. Nordsletten, I. Cappelen, and I. S. Kristiansen. Consequences of hip fracture on activities of daily life and residential needs. *Osteoporosis International*, 15(7):567–574, July 2004. doi: 10.1007/s00198-003-1583-0.

[3] P. Kannus, J. Parkkari, H. Sievänen, A. Heinonen, I. Vuori, and M. Järvinen. Epidemiology of hip fractures. *Bone*, 81(1 Suppl):57S–63S, January 1996. doi: 10.1016/8756-3282(95)00381-9.

[4] P. Carpintero, J. R. Caeiro, R. Carpintero, A. Morales, S. Silva, and M. Mesa. Complications of hip fractures: a review. *World Journal of Orthopedics*, 5(4):402–411, September 2014. doi: 10.5312/wjo.v5.i4.402.

[5] S. Eberle, C. Gerber, G. von Oldenburg, F. Högel, and P. Augat. A biomechanical evaluation of orthopaedic implants for hip fractures by finite element analysis and in-vitro tests. *Proceedings of the Institution of Mechanical Engineers, Part H*, 224(10):1141–1152, October 2010. doi: 10.1243/09544119JEIM799.

[6] A. Arias-Blanco, M. Marco, E. Giner, M. H. Miguélez, J. R. Caeiro-Rey, and R. Larraínzar-Garijo. The cut-out phenomenon in intertrochanteric femur fracture: analysis using a finite element model. *Revista de Osteoporosis y Metabolismo Mineral*, 13(1):21–31, 2021. doi: 10.4321/S1889-836X2021000100005.

[7] A. J. Bojan, C. Beimel, G. Taglang, D. Collin, C. Ekholm, and A. Jönsson. Critical factors in cut-out complication after gamma nail treatment of proximal femoral fractures. *BMC Musculoskeletal Disorders*, 14(1), January 2013. doi: 10.1186/1471-2474-14-1.

[8] H. Andruszkow, M. Frink, C. Frömke, A. Matityahu, C. Zeckey, P. Mommsen, S. Suntardjo, C. Krettek, and F. Hildebrand. Tip apex distance, hip screw placement, and neck shaft angle as potential risk factors for cut-out failure of hip screws after surgical treatment of intertrochanteric fractures. *International Orthopaedics*, 36(11):2347–2354, November 2012. doi: 10.1007/s00264-012-1636-0.

[9] K. K. Hsueh, C. K. Fang, C. M. Chen, Y. P. Su, H. F. Wu, and F. Y. Chiu. Risk factors in cutout of sliding hip screw in intertrochanteric fractures: an evaluation of 937 patients. *International Orthopaedics*, 34:1273–1276, September 2010. doi: 10.1007/s00264-009-0866-2.

[10] T. Fujii, S. Nakayama, M. Hara, W. Koizumi, T. Itabashi, and M. Saito. Tip-apex distance is most important of six predictors of screw cutout after internal fixation of intertrochanteric fractures in women. *JB & JS Open Access*, 2(4), December 2017. doi: 10.2106/JBJS.OA.16.00022.

[11] R. Valentini, M. Martino, G. Piovan, G. Fabrizio, and G. Fancellu. Proximal cut-out in pertrochanteric femural fracture. *Acta Biomedica*, 85(2):144–151, August 2014.

[12] M. Büyükkuscu, S. Basilgan, A. Misir, A. Polar, and H. Basar. Factors associated with the development of screw cut-out after the fixation of intertrochanteric femoral fractures with a proximal femoral nail. *Journal of Health Sciences and Medicine*, 4(2):170–175, March 2021. doi: 10.32322/jhsm.860548.

[13] P. Y. Lee, K. J. Lin, H. W. Wei, J. J. Hu, W. C. Chen, C. L. Tsai, and K. P. Lin. Biomechanical effect of different femoral neck blade position on the fixation

of intertrochanteric fracture: a finite element analysis. *Biomedical Engineering*, 61(3), September 2015. doi: 10.1515/bmt-2015-0091.

[14] T. Celik, I. Mutlu, A. Ozkan, and Y. Kisioglu. Comparison of the lag screw placements for the treatment of stable and unstable intertrochanteric femoral fractures regarding trabecular bone failure. *Journal of Medical Engineering*, 2016, November 2016. doi: 10.1155/2016/5470798.

[15] C. Liang, R. Peng, N. Jiang, G. Xie, L. Wang, and B. Yu. Intertrochanteric fracture: Association between the coronal position of the lag screw and stress distribution. *Asian Journal of Surgery*, 41(3):241–249, May 2018. doi: 10.1016/j.asjsur.2017.02.003.

[16] J. M. Goffin, P. Pankaj, and A. H. Simpson. The importance of lag screw position for the stabilization of trochanteric fractures with a sliding hip screw: A subject-specific finite element study. *Journal of Orthopaedic Research*, 31(4):596–600, October 2012. doi: 10.1002/jor.22266.

[17] C. Quental, S. Vasconcelos, J. Folgado, and F. Guerra Pinto. Influence of the PFNA screw position on the risk of cut-out in an unstable intertrochanteric fracture: a computational analysis. *Medical Engineering and Physics*, 97:70–76, October 2021. doi: 10.1016/j.medengphy.2021.10.001.

[18] M. R. Baumgaertner, S. L. Curtin, D. M. Lindskog, and J. M. Keggi. The value of the tip-apex distance in predicting failure of fixation of peritrochanteric fractures of the hip. *The Journal of Bone and Joint Surgery. American volume*, 77(7):1058–1064, July 1995. doi: 10.2106/00004623-199507000-00012.

[19] R. Hambli. A quasi-brittle continuum damage finite element model of the human proximal femur based on element deletion. *Medical & Biological Engineering & Computing*, 51(1-2):219–231, November 2013. doi: 10.1007/s11517-012-0986-5.

[20] U. Wolfram, H. J. Wilke, and P. K. Zysset. Damage accumulation in vertebral trabecular bone depends on loading mode and direction. *Journal of Biomechanics*, 44(6):1164–1169, April 2011. doi: 10.1016/j.jbiomech.2011.01.018.

[21] H. H. Bayraktar, E. F. Morgan, G. L. Niebur, G. E. Morris, E. K. Wong, and T. M. Keaveny. Comparison of the elastic and yield properties of human femoral trabecular and cortical bone tissue. *Journal of Biomechanics*, 37(1):27–35, January 2004. doi: 10.1016/S0021-9290(03)00257-4.

[22] D. van Embden, M. S. Gaston, L. A. Bailey, and A. H. Simpson. Trochanteric femoral fracture classification: Relevance of the fracture line angle, a radiological study. *International Journal of Orthopaedics*, 2(2):250–255, April 2015. doi: 10.6051/j.issn.2311-5106.2015.02.55.

[23] DePuy Synthes Trauma. *PFNA. With Augmentation Option - Surgical Technique Guide*, 2020. Available from: https://ifu.depuysynthes.com/.

[24] B. L. Riggs, J. Melton III, R. A. Robb, J. J. Camp, E. J. Atkinson, J. M. Peterson, P. A. Rouleau, C. H. McCollough, M. L. Bouxsein, and S. Khosla. Population-based study of age and sex differences in bone volumetric density, size, geometry, and structure at different skeletal sites. *Journal of Bone and Mineral Research*, 19(12):1945–1954, December 2004. doi: 10.1359/jbmr.040916.

[25] C. Quental, J. Folgado, M. Comenda, J. Monteiro, and M. Sarmento. Primary stability analysis of stemless shoulder implants. *Medical Engineering & Physics*, 81:22–29, July 2020. doi: 10.1016/j.medengphy.2020.04.009.

[26] S. Gupta, F. C. T. van der Helm, and F. van Keulen. The possibilities of uncemented glenoid component—a finite element study. *Clinical Biomechanics*, 19(3):292–302, March 2004. doi: 10.1016/j.clinbiomech.2003.12.002.

[27] E. F. Morgan, H. H. Bayraktar, and T. M. Keaveny. Trabecular bone modulus–density relationships depend on anatomic site. *Journal of Biomechanics*, 36:897–904, July 2003. doi: 10.1016/S0021-9290(03)00071-X.

[28] S. Sowmianarayanan, A. Chandrasekaran, and R. Krishna Kumar. Finite element analysis of a subtrochanteric fractured femur with dynamic hip screw, dynamic condylar screw, and proximal femur nail implants – a comparative study. *Proceedings of the Institution of Mechanical Engineers, Part H*, 222(1):117–127, February 2008. doi: 10.1243/09544119JEIM156.

[29] M. O. Heller, G. Bergmann, J. P. Kassi, L. Claes, N. P. Haas, and G. N. Duda. Determination of muscle loading at the hip joint for use in pre-clinical testing. *Journal of Biomechanics*, 38(5):1155–1163, May 2005. doi: 10.1016/j.jbiomech.2004.05.022.

[30] G. Bergmann, F. Graichen, and A. Rohlmann. Hip joint loading during walking and running, measured in two patients. *Journal of Biomechanics*, 26(8):969–990, August 1993. doi: 10.1016/0021-9290(93)90058-m.

[31] P. Helwig, G. Faust, U. Hindenlang, A. Hirschmüller, L. Konstantinidis, C. Bahrs, N. Südkamp, and R. Schneider. Finite element analysis of four different implants inserted in different positions to stabilize an idealized trochanteric femoral fracture. *Injury*, 40(3):288–295, March 2009. doi: 10.1016/j.injury.2008.08.016.

[32] S. Vasconcelos. Influence of the femoral head screw position on the risk of cut out in trochanteric fractures: a computational analysis. Master's thesis, Instituto Superior Técnico, September 2020.

[33] M. N. Konya and Ö. Verim. Numerical optimization of the position in femoral head of proximal locking screws of Proximal Femoral Nail system; biomechanical study. *Balkan Medical Journal*, 34(5):425–431, September 2017. 10.4274/balkanmedj.2016.0732.

[34] M. Nayak, R. Yadav, V. Ganesh, and V. Digge. An unusual case of femoral head perforation following fixation with proximal femoral nail antirotation (PFNA-II) for an unstable intertrochanteric fracture: Case report and literature review. *Trauma Case Reports*, 20, February 2019. doi: 10.1016/j.tcr.2019.100178.

[35] L. Murena, A. Moretti, F. Meo, E. Saggioro, G. Barbati, C. Ratti, and G. Canton. Predictors of cut-out after cephalomedullary nail fixation of pertrochanteric fractures: a retrospective study of 813 patients. *Archive of Orthopaedic and Trauma Surgery*, 138(3):351–359, March 2018. doi: 10.1007/s00402-017-2863-z.

[36] K. De Bruijn, D. den Hartog, W. Tuinebreijer, and G. Roukema. Reliability of predictors for screw cutout in intertrochanteric hip fractures. *The Journal of Bone and Joint Surgery. American volume*, 94(14):1266–1272, July 2012. doi: 10.2106/JBJS.K.00357.

[37] F. Guerra Pinto, P. Dantas, R. Moreira, R. Mamede, and L. Branco Amaral. Complications relating to accuracy of reduction of intertrochanteric fractures treated with a compressive hip screw. *Hip International*, 20(2):221–228, April 2010. doi: 10.1177/112070001002000213.

[38] P. Bandeira. A continuum-damage model for advanced composites. Master's thesis, Faculty of Engineering of the University of Porto, August 2005.